International Journal of
Molecular Sciences

MDPI

Article

Macrophage-Associated CXCL3 and IL1RN as Candidate Genes Linked to Adipose Inflammation and Metabolic Dysfunction in Obesity

Kemin Yan †, Gang Yuan, Xiangbin Zhong †, Chen Li, Hua Yin, Meilin Ding, Wen He, Lei Su, Jin Li and Yingying Gong *

Department of Geriatrics, Department of Private Medical Center, The First Affiliated Hospital of Sun Yat-sen University, Guangzhou 510080, China; yankm3@mail.sysu.edu.cn (K.Y.); yuangang@mail.sysu.edu.cn (G.Y.); zhongxb3@alumni.sysu.edu.cn (X.Z.); lichen28@mail.sysu.edu.cn (C.L.); yinh37@mail2.sysu.edu.cn (H.Y.); dingmeil@mail.sysu.edu.cn (M.D.); hewen@mail.sysu.edu.cn (W.H.); sulei3@mail.sysu.edu.cn (L.S.); lijin8@mail.sysu.edu.cn (J.L.)
* Correspondence: gongyy5@mail.sysu.edu.cn; Tel.: +86-020-87755766-8650
† These authors contributed equally to this work.

Abstract

Insulin resistance (IR) is a central pathophysiological feature of obesity-related metabolic disorders, yet the macrophage subsets and mediators that drive IR in obese adipose tissue remain unclear. We used bulk transcriptomic data from an insulin-resistant versus insulin-sensitive cohort (GSE20950) to guide Scissor-based mapping of single-cell RNA sequencing data from human adipose tissue, and feature gene identification and validation were then performed in two further datasets assessing obesity status (GSE162653) and metabolic health status among obese individuals (GSE152991), respectively. High-dimensional weighted gene co-expression network analysis (hdWGCNA), differential expression, protein–protein interaction, and machine learning analyses were used to identify feature genes, whereas Gene Set Enrichment Analysis, immune infiltration, cell–cell communication, and virtual knockout analyses were used for functional characterization. Adipose tissue mRNA levels of IL1RN and CXCL3 were significantly higher in mice fed a high-fat diet than in normal-diet controls. Whole-field CXCL3 fluorescence intensity in adipose tissue sections did not differ significantly between the two groups ($p = 0.153$). Scissor analysis identified macrophages as the cell type most strongly associated with IR, with metabolically activated macrophages representing the most abundant subset (43.5%). Multi-layered screening identified CXCL3 and IL1RN as macrophage-associated candidate genes with increased expression in obesity and metabolically unhealthy obesity. In two independent HOMA-IR-defined cohorts, CXCL3 showed no statistically significant differences, whereas IL1RN was significantly elevated in only one cohort, providing limited evidence of an association with insulin resistance. GSEA suggested enrichment of IL1RN in major histocompatibility complex (MHC) class II antigen presentation, and virtual knockout of either gene perturbed MHC class II-related programs, a pathway previously implicated in adipose tissue inflammation. These computational findings raise a hypothesis regarding a possible association between CXCL3/IL1RN and antigen-presentation processes and do not establish a functional role for either gene in MHC class II antigen presentation. Immune infiltration analysis identified significant alterations in 21 immune cell populations, with both candidate genes showing strong correlations with macrophage abundance. The miRNA-mRNA-TF network analysis predicted hsa-miR-34a-5p as a potential upstream regulator of both CXCL3 and IL1RN. This study identifies CXCL3 and IL1RN as macrophage-associated candidate genes linked to adipose inflammation and metabolic dysfunction in obesity, with possible associations with insulin resistance, and highlights MAMs as the most abundant macrophage

Check for updates

Academic Editors: Antonio Maria Labate and Jean-François Tanti

Received: 19 September 2026
Revised: 15 November 2026
Accepted: 16 November 2026
Published: 23 November 2026

Copyright: © 2026 by the authors. Licensee MDPI, Basel, Switzerland. This article is an open access article distributed under the terms and conditions of the Creative Commons Attribution (CC BY) license.

subset. The convergence of IL1RN enrichment and virtual knockout results on MHC class II-related programs suggests a potential association between these candidate genes and antigen-presentation processes in obese adipose tissue. The proposed hsa-miR-34a-5p-CXCL3/IL1RN axis remains hypothetical and requires experimental validation.

Keywords: obesity; insulin resistance; macrophages; single-cell RNA sequencing; Scissor analysis; CXCL3; IL1RN

1. Introduction

Obesity is increasingly recognized as a chronic, multifactorial, and progressive disease characterized by excessive accumulation of body fat that poses a significant threat to global health [1]. It is linked to a variety of complications, such as type 2 diabetes, cardiovascular disease, obstructive sleep apnea, osteoarthritis, and cancers [2]. It has been forecast that the overall population of adults experiencing life with overweight and obesity will reach 3.80 billion by 2050, over half of the anticipated global adult population [3]. The development of obesity is characterized by a multifaceted interaction among environmental, physiological, genetic, and behavioral determinants [4], but a critical unifying mechanism linking obesity to its metabolic complications is insulin resistance. Insulin resistance is defined by a diminished sensitivity of insulin-responsive tissues to normal physiological concentrations of insulin [5]. In obesity, insulin resistance is driven by dysfunction in adipose tissue, persistent low-grade inflammation, and oxidative stress [5]. Adipose tissue is a dynamic metabolic organ comprising diverse cell types, including adipocytes, macrophages, T lymphocytes, fibroblasts, endothelial cells, adipose-derived stem and progenitor cells, neutrophils, and B lymphocytes, whose interactions collectively govern the tissue's physiological and pathological roles [6]. Among these cell types, macrophages are particularly critical. Excess nutrient intake induces low-grade chronic inflammation in adipose tissue, which in turn promotes macrophage accumulation and the development of insulin resistance [7].

Recent studies using single-cell transcriptomics have shown that adipose tissue macrophages (ATMs) exhibit far greater heterogeneity than the traditional M1/M2 paradigm suggests. Several metabolically distinct ATM subsets have been identified in obese adipose tissue, including crown-like structure macrophages (CLS) that localize around dying adipocytes to clear cellular debris, lipid-associated macrophages (LAMs) that facilitate lipid catabolism and tissue remodeling, and sympathetic neuron-associated macrophages (NAMs/SAMs) that import and degrade norepinephrine, thereby suppressing thermogenesis [8,9]. These subsets can exert divergent metabolic effects. LAMs may protect against adipocyte hypertrophy, whereas NAMs can promote obesity by limiting sympathetic catecholamine signaling. Additionally, metabolically activated macrophages (MAMs), a newly characterized subset induced by exposure to elevated concentrations of glucose, insulin, and palmitate, have been shown to upregulate inflammatory markers and genes involved in lipid metabolism during diet-induced obesity [10]. Despite these advances, the specific macrophage subsets and molecular mediators that directly drive obesity-associated insulin resistance remain incompletely understood, and few studies have systematically linked these subsets to sample-level insulin resistance phenotypes using integrative computational approaches [11].

Although bulk transcriptomic studies have identified numerous differentially expressed genes associated with obesity and insulin resistance, they average gene expression across all cell types, thereby masking cell-type-specific signals which are essential for analyzing the underlying mechanisms of diseases. CXCL3, a C-X-C motif chemokine, promotes

leukocyte recruitment and has been implicated in inflammatory responses in adipose tissue, whereas IL1RN encodes the interleukin-1 receptor antagonist that counter-regulates IL-1 signaling and participates in inflammatory homeostasis. Both factors have been reported to be upregulated in obese adipose tissue [12,13], yet direct experimental evidence for their combined action or synergistic regulation in inflammation remains limited. In the present study, we examined CXCL3 and IL1RN as macrophage-associated candidate genes and explored the molecular programs associated with each gene, including those shared by both, without presupposing a synergistic interaction. Single-cell RNA sequencing (scRNA-seq) resolves cellular heterogeneity but typically involves limited sample sizes and lacks direct linkage between individual cells and sample-level phenotypes. The Scissor algorithm addresses this limitation by integrating bulk phenotypic data with single-cell transcriptomic data through a regression-based framework that identifies phenotype-associated cell subpopulations without requiring a priori clustering [11]. This approach has been successfully applied in cancer immunology and neurodegenerative diseases. However, its application to insulin resistance in obese adipose tissue remains relatively limited.

In this study, we integrated the Scissor algorithm with single-cell transcriptomic data to systematically identify key cell populations and candidate genes associated with insulin resistance in obese adipose tissue. We further investigated the roles of these candidate genes in modulating immune responses and key signaling pathways and shaping cellular functions. At the single-cell level, cell–cell communication analysis and virtual knockout analysis using the scTenifoldKnk tool [14] were performed to evaluate the regulatory effects of these candidate genes on downstream signaling pathways. The expression of the identified candidate genes was subsequently examined in a mouse model of high-fat diet-induced obesity. This integrative strategy aimed to bridge the gap between cellular heterogeneity and clinical phenotypes, providing testable hypotheses regarding macrophage-associated insulin resistance and nominating candidates for further mechanistic investigation.

2. Results

2.1. Annotation of Five Cell Types

In the GSE129363 single-cell transcriptomics dataset, after quality control, the dataset contained 13,384 cells and 33,694 genes (Supplementary Figure S1A). Next, 2000 HVGs were identified, and the top 10 HVGs were labeled (Supplementary Figure S1B). PCA was performed, and the top 10 PCs were selected for further analysis (Supplementary Figure S1C). The cells were divided into 13 clusters. Clusters 0, 2, 3, and 10 expressed the adipose progenitor/stromal markers CFD, MGP, APOD, CXCL14, and WISP2 and were annotated as adipose stromal/progenitor cells (ASP); the remaining clusters were assigned to macrophages, pericytes, T cells, and B cells (Figure 1A). The expression of the markers used for annotation is shown as a dot plot (Figure 1B). Single-cell expression of each annotation marker is shown in Supplementary Figure S2. Scissor+ cells exhibited the highest proportion in macrophages, indicating a strong association between macrophages and insulin resistance. Therefore, macrophages were defined as key cells (Figure 1C).

2.2. Identification of 400 Key Module Genes

To identify co-expressed gene modules in key cells at the single-cell level, hdWGCNA analysis was performed on the GSE129363 dataset. The key cells were divided into 11 subclusters (Figure 2A). The hdWGCNA analysis showed that the optimal soft threshold (power) was determined to be 4, where $R^2 > 0.8$ (Figure 2B). Next, a co-expression matrix was established, and 4 modules were determined (Figure 2C). The top 100 genes based on kME values in each module were selected as key module genes, containing a total of 400 genes. The top 10 genes in the 4 modules were displayed (Figure 2D). Module 3 was

correlated with Module 2 and Module 1 (Figure 2E). A total of 4 modules exhibited high activity in key cell subclusters (Figure 2F).

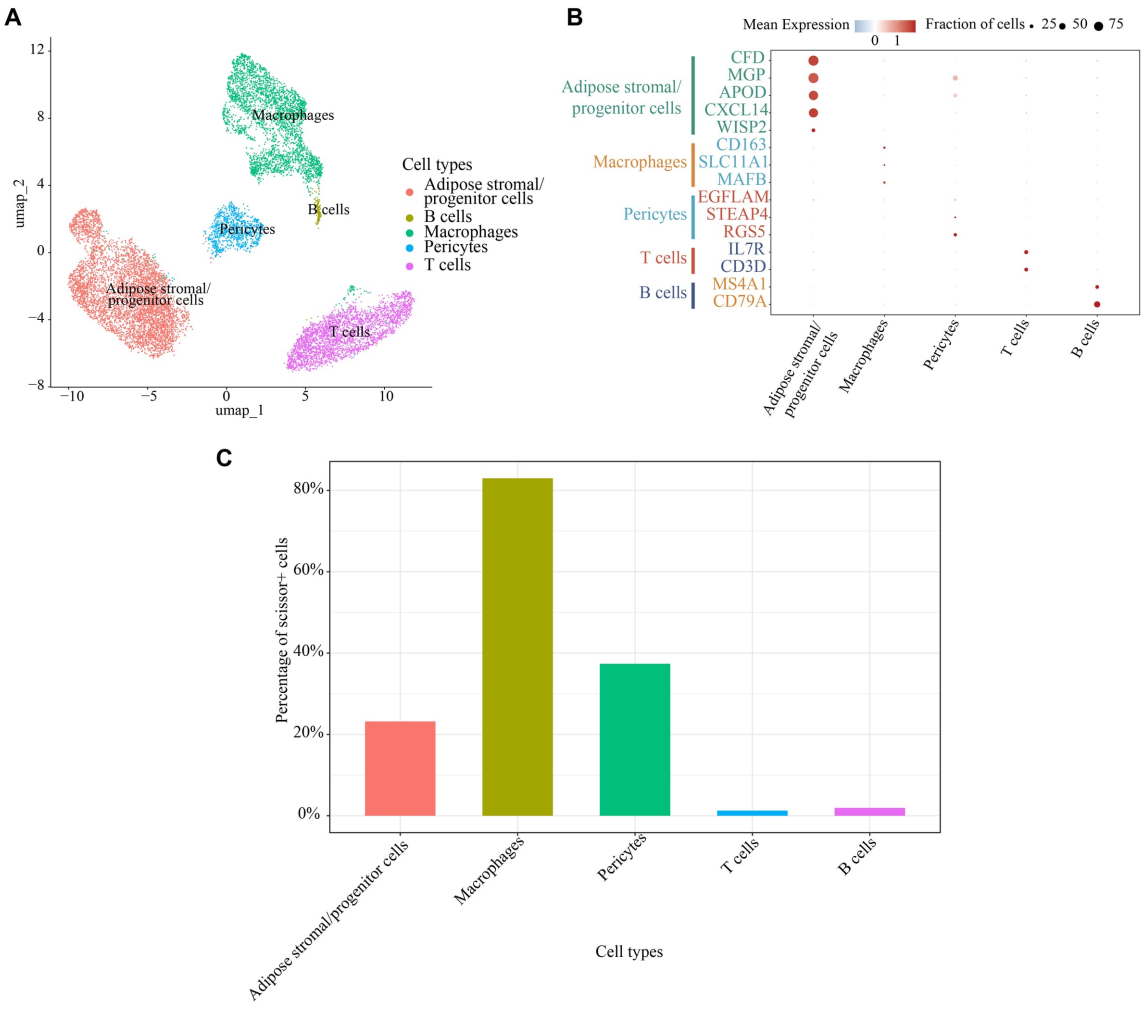

Figure 1. Annotation of five cell types. (**A**) UMAP of the five annotated cell types (adipose stromal/progenitor cells, macrophages, pericytes, T cells, and B cells). (**B**) Dot plot of the markers used for annotation. (**C**) Proportion of Scissor+ cells in the five cell types.

2.3. Subsets and Pseudotime Trajectory Analysis of Macrophages

The key macrophages were divided into 6 key cell subsets, including crown-like structure macrophages (CLS), vascular-associated macrophages (VAMs), lipid-associated macrophages (LAMs), metabolically activated macrophages (MAMs), sympathetic neuron-associated macrophages (NAMs), and proliferative macrophages (ProMac) (Figure 3A,B). Among them, MAMs accounted for a relatively high proportion in the overall samples (Figure 3C). No marked difference in the abundance of the six macrophage subsets was observed between diabetic and non-diabetic samples (Figure 3D); this comparison was exploratory and was not adjusted for clinical confounders.

Pseudotime analysis revealed that the differentiation trajectories of macrophages advanced from a deep purple to a light yellow gradient (Figure 3E). The developmental stages of the cells were segmented into 45 distinct intervals, each represented by a unique color, with stage 1 denoting the early phase of differentiation (Figure 3F). Key cell subcluster 4 was located at the early stage of cell differentiation (Figure 3G). These findings delineated the differentiation trajectory of macrophage subclusters.

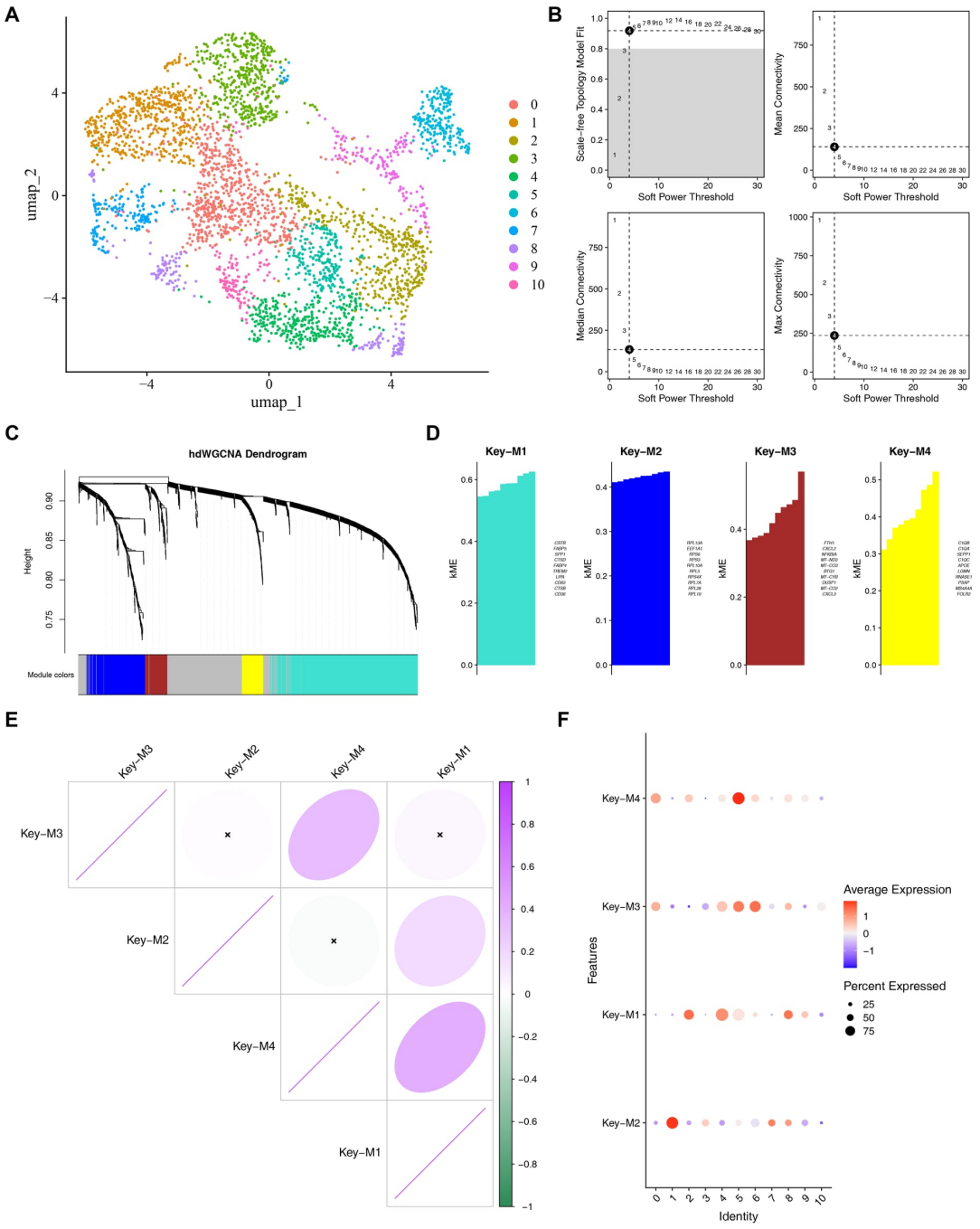

Figure 2. Identification of 400 key module genes. (**A**) 11 key cell subclusters. (**B**) Soft-threshold selection. Numbers indicate the tested soft-thresholding powers. The black circle and vertical dashed line mark the selected power ($\beta = 4$), and the horizontal dashed lines indicate the corresponding values of each metric. (**C**) Identification of 4 modules. (**D**) Top 10 genes of each module. (**E**) Correlations between modules. (**F**) Module activity in key cell subclusters. Analyses were restricted to the key cells (macrophages) from the 13 subcutaneous adipose tissue samples in GSE129363.

2.4. Exploring Cell Functions from Multiple Perspectives

Cell communication analysis indicated that macrophages engaged in autocrine signaling and communicated with ASP (Figure 4A,B). In addition, when macrophages served as signal senders, the ligand-receptor pair between macrophages and ASP was identified as SPP1-CD44 (Figure 4C). These findings indicated selective macrophage-ASP crosstalk in the dataset.

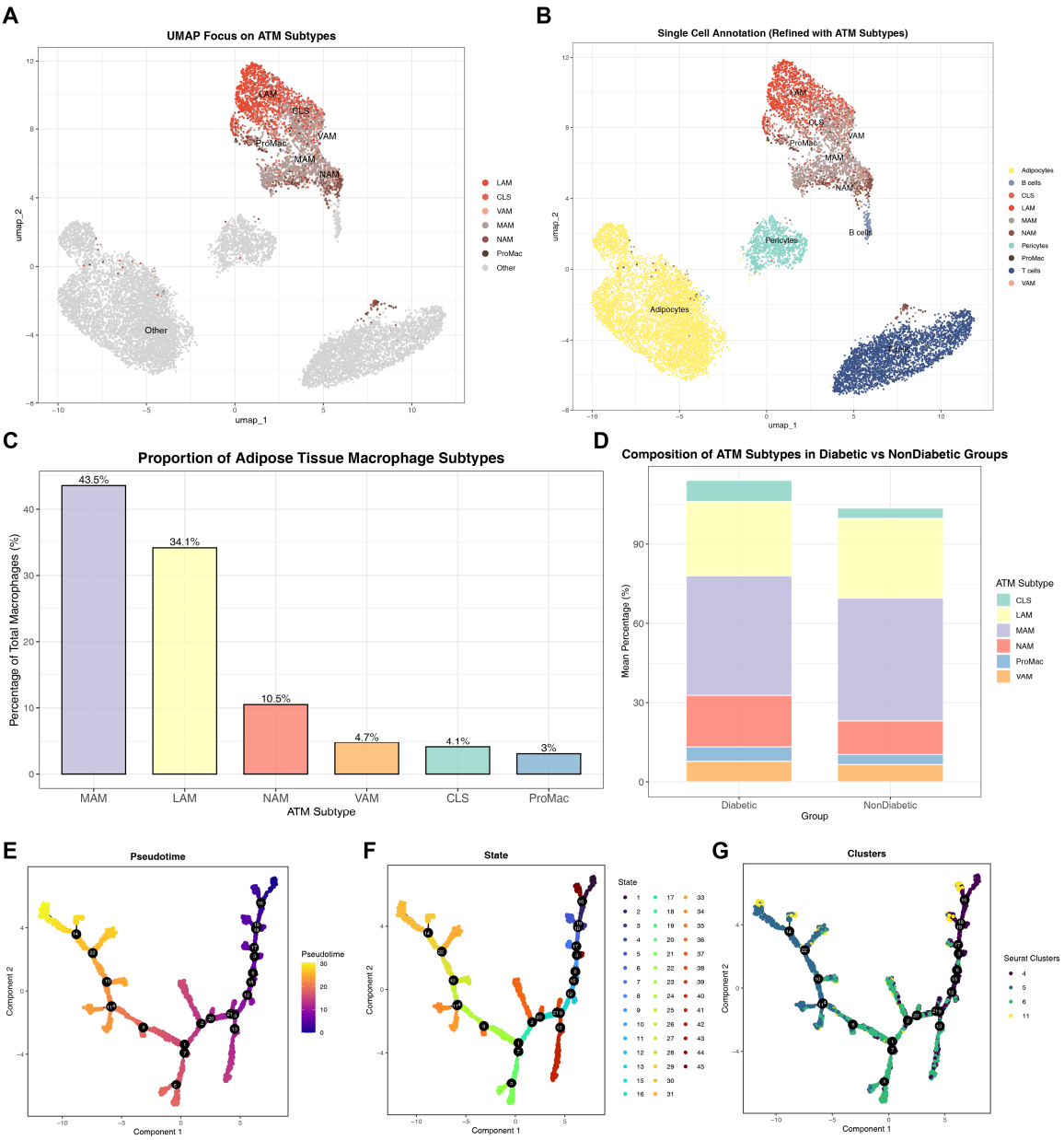

Figure 3. Subsets and pseudotime trajectory analysis of key cells. (**A**) The six key cell subtypes. (**B**) UMAP visualization of key cell subsets combined with other annotated cell types. (**C**) Proportions of key cell subsets in all samples. (**D**) Proportions of key cell subsets in the diabetic versus non-diabetic groups. (**E**) Trajectory plot of differences in cell differentiation pseudotime. (**F**) State diagrams of cell differentiation. (**G**) Key cell subcluster distribution profiles in the differentiation processes. UMAP embeddings were computed from 2000 highly variable genes and the top 10 principal components, and cell proportions were calculated per sample. Numbered black circles mark branch points along the inferred trajectory. In panel F, the numbers in the legend denote trajectory states.

The pathway of valine, leucine and isoleucine degradation was relatively enriched in cell subclusters 2, 4, 5, 6 and 8; tyrosine metabolism was relatively enriched in cell subcluster 6; tryptophan metabolism was relatively enriched in cell subclusters 4, 5 and 8; phenylalanine metabolism was relatively enriched in cell subclusters 0, 1, 2, 3, 7 and 10; oxidative phosphorylation was relatively enriched in cell subclusters 2, 4 and 8; lysine degradation was relatively enriched in cell subcluster 4; glycine, serine and threonine metabolism was relatively enriched in cell subclusters 2, 4, 5 and 8; fatty acid elongation was

relatively enriched in cell subclusters 2, 4, 5, 6 and 8; fatty acid degradation was relatively enriched in cell subclusters 4 and 8 (Figure 4D).

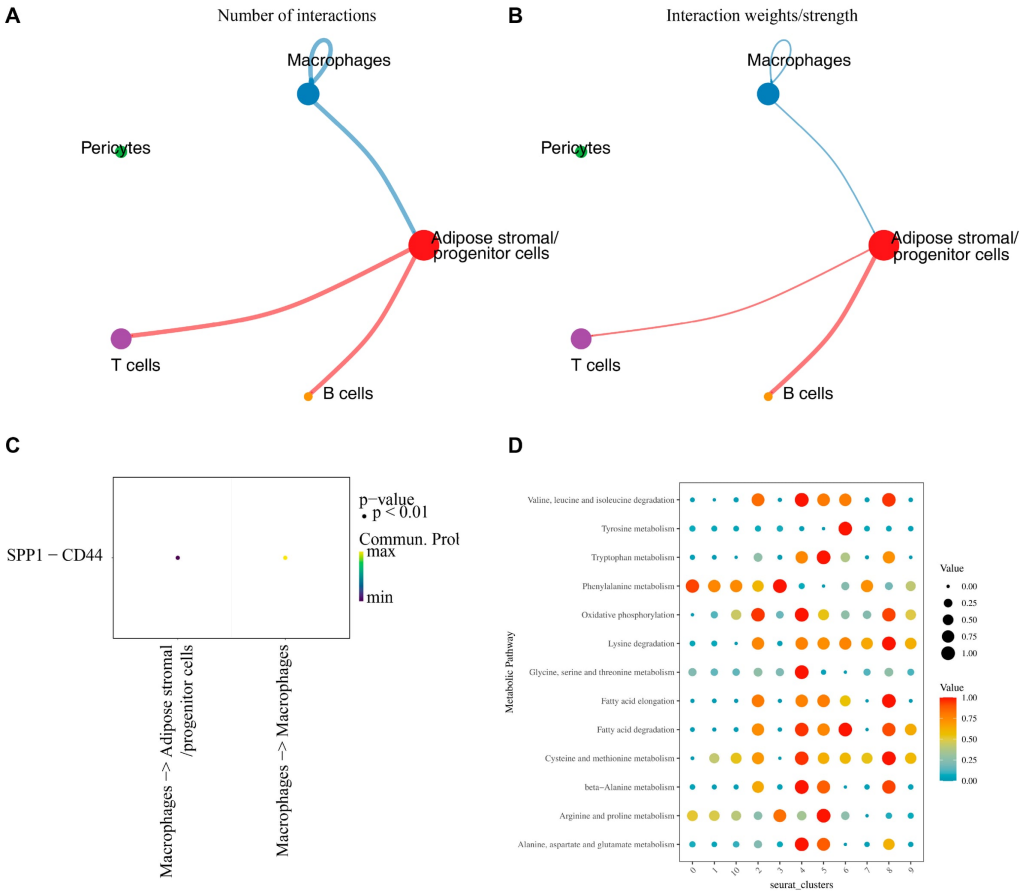

Figure 4. Cell–cell communication and metabolic activity of the key cell clusters. (**A**) Number of interactions among the five cell types. (**B**) Interaction strength among the five cell types. (**C**) Ligand-receptor pairs when macrophages act as signal senders, with SPP1-CD44 indicated. (**D**) Activity of metabolic pathways in key cell subclusters. Communication probabilities were computed with CellChat, and interactions with $p < 0.01$ are shown.

2.5. Identification of 12 Hub Genes

In the GSE162653 dataset, 899 bulk DEGs were identified, including 625 upregulated genes and 274 downregulated genes in the obesity group compared with the control group (Supplementary Figure S3A,B). By intersecting the bulk DEGs with key module genes, 35 overlapping genes were identified (Supplementary Figure S3C). All 35 overlapping genes were connected in the PPI network (Supplementary Figure S3D). Finally, the 12 genes of the top-ranked MCODE module were taken as hub genes, including MMP9, CXCL6, IL1RN, CCL3, CXCL9, IL10, CCL4, CCR1, CXCL2, CXCL3, CXCL1, and CD163.

2.6. Identification of CXCL3 and IL1RN as Candidate Genes

To further screen feature genes, three machine learning algorithms were applied. A total of 10 Boruta genes were obtained through Boruta analysis (Figure 5A). A total of 8 SVM-RFE genes were obtained through SVM-RFE analysis (Figure 5B). Additionally, 5 RF genes were obtained (Figure 5C). By intersecting Boruta genes, SVM-RFE genes, and RF genes, five feature genes, including MMP9, IL1RN, CCL3, CXCL1, and CXCL3, were identified (Figure 5D). Moreover, expression of the five feature genes in the discovery dataset (GSE162653) comparing obese patients with normal subjects, and in the valida-

tion dataset (GSE152991) comparing metabolically unhealthy with metabolically healthy obese patients, revealed that IL1RN and CXCL3 were significantly upregulated in both the obesity group and the metabolically unhealthy obesity group ($p < 0.05$, Figure 5E,F, Supplementary Table S2). Although IL1RN and CXCL3 were both upregulated in obesity, this co-directional change does not by itself indicate co-regulation or functional synergy between the two genes. These comparisons assess obesity status and metabolic health status among obese individuals, respectively, and do not by themselves establish IR specificity. Accordingly, among these feature genes, IL1RN and CXCL3 were retained as candidate genes supported by obesity status and metabolic health status; their IR linkage was derived from Scissor-guided mapping using GSE20950 and requires independent clinical validation.

To examine whether CXCL3 and IL1RN differ between insulin-resistant and insulin-sensitive states in independent cohorts, we analyzed two datasets with HOMA-IR-defined groups. In GSE101492 (40 insulin-sensitive vs. 40 insulin-resistant samples), both genes were higher in the insulin-resistant group, but the differences were not statistically significant (IL1RN, $p = 0.252$; CXCL3, $p = 0.248$; Supplementary Figure S4A). In GSE174475 (16 insulin-sensitive vs 27 insulin-resistant samples), IL1RN was significantly upregulated in the insulin-resistant group ($p = 4.37 \times 10^{-5}$), whereas CXCL3 showed a consistent but non-significant trend ($p = 0.123$; Supplementary Figure S4B). These results provided limited external support for the association of IL1RN with insulin resistance, whereas the evidence for CXCL3 remained inconclusive; neither gene was established as specific to insulin resistance.

2.7. Pathways Associated with Candidate Gene Expression and Virtual Knockout Analysis

GSEA revealed that IL1RN was enriched in 738 pathways, including "MHC class II antigen presentation" and "immunoregulatory interactions between a lymphoid and a non-lymphoid cell" (Figure 6A, Supplementary Table S3). CXCL3 was enriched in 807 pathways, including "interleukin 10 signaling" and "mitochondrial complex IV assembly" (Figure 6B, Supplementary Table S4).

Upon IL1RN virtual KO, the affected genes were significantly enriched for 320 GO terms, including major histocompatibility complex (MHC) class II protein complex binding and MHC class II receptor activity, and 47 KEGG pathways, including phagosome (Figure 6C,D, Supplementary Tables S5 and S6). After CXCL3 virtual KO, the perturbed genes were significantly enriched for 325 GO terms, including MHC class II protein complex binding and MHC class II receptor activity, and 38 KEGG pathways, including allograft rejection (Figure 6E,F, Supplementary Tables S7 and S8). These computational results indicate that immune-related pathways, including MHC class II-related programs, are enriched among genes perturbed by virtual knockout of IL1RN or CXCL3. They raise a hypothesis of a possible association with antigen-presentation processes but do not establish a functional regulatory role, which requires tissue-level co-localization and functional perturbation experiments.

2.8. Association of Candidate Genes with the Immune Microenvironment and miRNA-TF Regulatory Network

The xCell enrichment scores for 21 immune cell types, including M1 macrophages and B cells, differed significantly between the obesity group and the control group ($p < 0.05$) (Figure 7A). Macrophage scores showed the strongest positive correlation with M2 macrophage scores (correlation coefficient, cor = 0.96, $p < 0.0001$) (Figure 7B). In addition, IL1RN showed the strongest positive correlation with M2 macrophages (cor = 0.93, $p < 0.0001$), and CXCL3 showed the strongest positive correlation with macrophages (cor = 0.75, $p < 0.0001$) (Figure 7C, Supplementary Table S9). These results indicated that candidate gene expression was associated with immune cell enrichment patterns in obesity.

The network analysis predicted hsa-miR-34a-5p and hsa-miR-130a-3p as potential upstream regulators of both IL1RN and CXCL3. The network also included predicted links between each candidate gene and the transcription factors MTF1 and ETV3L (Figure 7D). The proposed hsa-miR-34a-5p-CXCL3/IL1RN axis remains hypothetical and requires experimental validation.

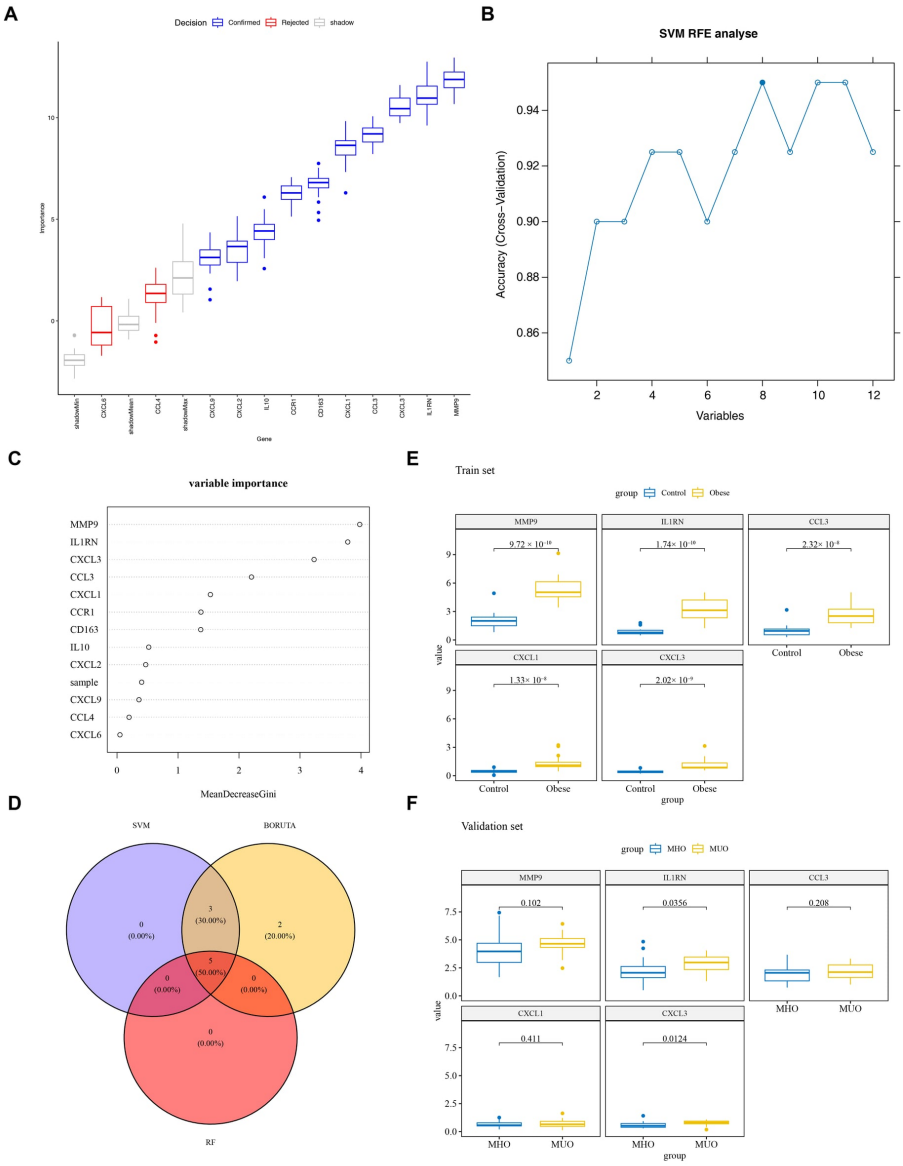

Figure 5. Identification of CXCL3 and IL1RN as candidate genes. (**A**) Boruta analysis for Boruta gene identification. Blue, red, and gray indicate confirmed features, rejected features, and shadow features, respectively. (**B**) SVM-RFE analysis for SVM-RFE gene identification. The filled circle marks the selected eight-gene subset, and open circles indicate the other subset sizes evaluated by cross-validation. (**C**) RF analysis for RF gene identification. Open circles indicate random forest variable importance scores. (**D**) Identification of feature genes by intersecting Boruta genes, SVM-RFE genes, and RF genes. (**E**) Expression of the feature genes in the discovery dataset (GSE162653) comparing obese patients with normal subjects. (**F**) Expression of the feature genes in the validation dataset (GSE152991) comparing metabolically unhealthy obese patients with metabolically healthy obese patients. Boxplots show the median and interquartile range; whiskers extend to 1.5× the interquartile range; each point represents one sample. *p*-values were calculated using the Wilcoxon test. These comparisons evaluate obesity status and metabolic health status among obese individuals, respectively, rather than insulin resistance per se. $n = 20$ samples per group in (**E**) and $n = 34$ samples in (**F**).

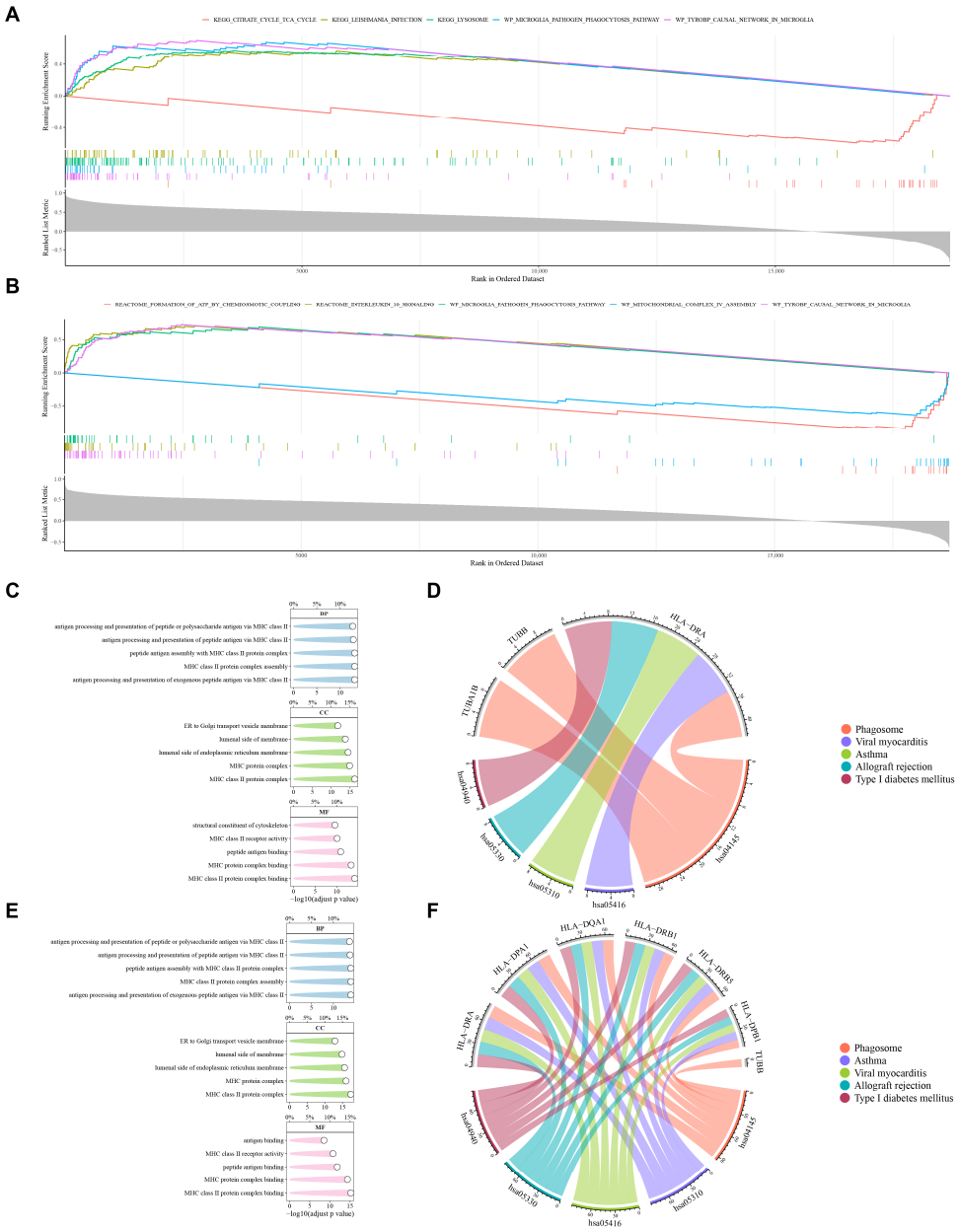

Figure 6. Pathways associated with candidate gene expression and virtual knockout analysis. (**A**) Top 5 pathways enriched by IL1RN. (**B**) Top 5 pathways enriched by CXCL3. (**C**,**D**) GO and KEGG pathways enriched by genes affected following virtual knockout analysis on IL1RN. (**E**,**F**) GO and KEGG pathways enriched by genes affected following virtual knockout analysis on CXCL3. NES, normalized enrichment score; FDR, false discovery rate; pathways are shown at $|NES| > 1$, FDR < 0.25 and $p < 0.05$.

2.9. Enrichment Characteristics of Macrophage-Related Genes

GSEA was performed in macrophages with detectable CXCL3 expression. Pathways related to pro-inflammatory and secretory functions, including an overview of pro-inflammatory and pro-fibrotic mediators, secreted factors, inflammatory response Lps up, and SenMayo, were significantly upregulated. In contrast, pathways such as eukaryotic translation initiation/elongation, mycosis fungoides CD4 up, rRNA processing, and regulation of expression of slits and robos were downregulated. These results indicated that macrophages with detectable CXCL3 expression showed enrichment of pro-inflammatory and secretory pathways, accompanied by suppression of translation- and metabolism-

related pathways (Supplementary Figure S5A). Meanwhile, macrophages with detectable IL1RN expression showed enrichment of pathways associated with extracellular matrix organization and remodeling, while translation-related pathways were suppressed, suggesting a matrix regulatory and pro-remodeling functional profile (Supplementary Figure S5B).

2.10. Expression of IL1RN and CXCL3 in Adipose Tissue of HFD-Induced Obese Mice

Subsequently, animal experiments were conducted to examine IL1RN and CXCL3 expression in adipose tissue of HFD-induced obese mice. RT-qPCR analysis showed significantly increased mRNA levels of IL1RN and CXCL3 in obese mice compared with lean controls (Figure 8A,B, $p < 0.05$). Immunofluorescence staining was performed to qualitatively assess the spatial distribution of IL1RN signals relative to F4/80-positive cells (Figure 8C). Whole-field fluorescence quantification revealed significantly higher IL1RN staining intensity in the HFD group (Figure 8D, $p < 0.05$). Similarly, the spatial distribution of CXCL3 signals relative to F4/80-positive cells was qualitatively examined (Figure 8E), while whole-field CXCL3 fluorescence intensity showed a non-significant increasing trend in the HFD group (Figure 8F, $p = 0.153$). These quantitative measurements reflected tissue-level staining rather than macrophage-specific protein expression. Overall, the findings provided mRNA-level support for the bioinformatics results, whereas the cellular sources and protein-level changes require further validation.



Figure 7. Candidate gene-associated immune cells and miRNA-TF regulatory network. (**A**) Box plot of differential xCell enrichment scores for 34 immune cell types; 21 immune cell types showed significant between-group differences ($p < 0.05$). (**B**) Correlations among immune cell types with differential xCell enrichment scores ($|cor| > 0.30$, $p < 0.05$). (**C**) Correlations between the candidate genes and immune cell types with differential xCell enrichment scores ($|cor| > 0.30$, $p < 0.05$). **** $p < 0.0001$, *** $p < 0.001$, ** $p < 0.01$, * $p < 0.05$; ns, not statistically significant. (**D**) Predicted miRNA-mRNA-TF regulatory network for IL1RN and CXCL3. Between-group differences in xCell enrichment scores in (**A**) were assessed using the Wilcoxon test, and Spearman correlations are shown in (**B**,**C**).

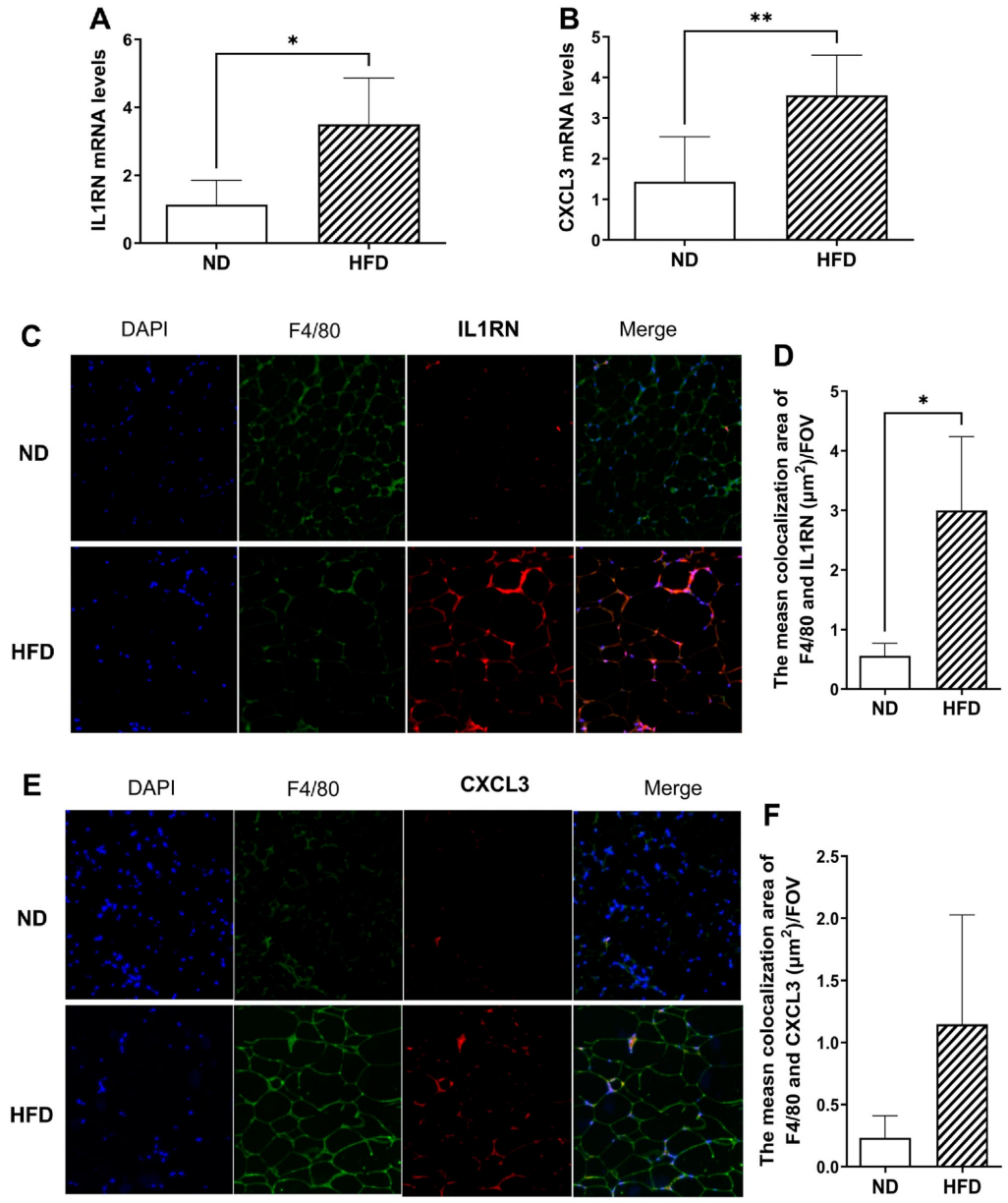

Figure 8. Expression of IL1RN and CXCL3 in adipose tissue of HFD-induced obese mice. Mice were fed a normal diet (ND; $n = 3$) or a high-fat diet (HFD; $n = 4$) for 24 weeks. (**A**,**B**) Relative mRNA expression of IL1RN and CXCL3 determined by RT-qPCR. (**C**,**E**) Representative immunofluorescence images showing DAPI (blue), F4/80 (green), and IL1RN or CXCL3 (red). Merged images were used for qualitative assessment of signal distribution relative to F4/80-positive cells. (**D**,**F**) Quantification of whole-field IL1RN and CXCL3 fluorescence intensity, respectively, rather than fluorescence restricted to F4/80-positive regions. Two sections and five fields per section were analyzed for each animal, and field measurements were averaged to obtain one value per animal. Data are presented as mean ± SD. Group comparisons were performed using the *t*-test. * $p < 0.05$, ** $p < 0.01$ versus ND. CXCL3 whole-field fluorescence intensity did not differ significantly between groups ($p = 0.153$).

3. Discussion

In obesity, dysfunctional adipose tissue plays a critical role in the onset of insulin resistance [15]. Immune cell accumulation within the adipose microenvironment is a primary driver of insulin resistance and metabolic dysfunction, wherein infiltrating immune cells, adipocytes, and stromal cells collectively produce pro-inflammatory cytokines and chemokines that disrupt systemic homeostasis [16]. In the present study, through a multi-

dimensional analytical framework integrating Scissor, hdWGCNA, machine learning, and functional genomics, we identified CXCL3 and IL1RN as macrophage-associated candidate genes linked computationally to obesity-related insulin resistance. Macrophages emerged as the key cell type, with MAMs representing the most abundant subset. Both candidate genes showed convergence in MHC class II-related programs: GSEA suggested enrichment for IL1RN, and virtual knockout of either gene perturbed MHC-II-related gene programs, raising the hypothesis, rather than establishing a mechanism, that macrophage-derived mediators may be associated with adaptive immune responses in obese adipose tissue. These findings provide a multi-level perspective on the candidate genes, pathways, and cellular mechanisms underlying obesity-related insulin resistance.

C-X-C motif chemokine 3 (CXCL3), a member of the C-X-C chemokine subfamily, acts as a potent chemoattractant for neutrophils and coordinates leukocyte recruitment while inducing inflammatory responses [12]. Interleukin-1 receptor antagonist (IL-1RA), encoded by the IL1RN gene, is a natural inhibitor of IL-1 signaling that regulates a wide range of IL-1-mediated immune and inflammatory responses [17]. Scissor analysis linked macrophages to IR, and subsequent analyses identified CXCL3 and IL1RN as macrophage-associated candidate genes. Expression of both genes was significantly higher in individuals with obesity than in controls and significantly higher in metabolically unhealthy individuals with obesity than in their metabolically healthy counterparts. In two independent HOMA-IR-defined cohorts, IL1RN expression was significantly higher in the insulin-resistant group in one cohort, whereas CXCL3 expression did not differ significantly in either cohort (Section 2.6). Adipose tissue mRNA levels of both genes were significantly higher in mice fed a high-fat diet than in normal-diet controls (Figure 8A,B). Representative merged images were used to qualitatively assess the spatial distribution of CXCL3 staining relative to F4/80-positive cells (Figure 8E). Whole-field CXCL3 fluorescence intensity in adipose tissue sections did not differ significantly between the two diet groups (Figure 8F, $p = 0.153$). The concurrent elevation of CXCL3 and IL1RN transcript levels in obese adipose tissue may reflect the coexistence of chemokine-driven inflammatory cell recruitment and a compensatory response that limits IL-1 signaling [13,18].

Consistent with our findings, previous studies have demonstrated that adipocytes from obese individuals exhibit significantly higher levels of CXCL3 [12]. Notably, a single-cell study integrating multiple scRNA-seq datasets identified CXCL3 as a characteristic marker gene of inflammatory macrophages, a subset enriched in obese human subcutaneous adipose tissue [19]. Additionally, adipocytes can produce CXCL3 via the STAT3 signaling pathway under inflammatory conditions, with CXCL3 exerting its effects through the CXCR2 receptor [20]. These findings collectively position CXCL3 at the intersection of adipocyte-macrophage crosstalk in obesity, although CXCL3-specific mechanistic studies remain lacking. Regarding IL1RN, serum IL-1RA levels show a graded increase with obesity severity and glucose intolerance, and visceral adipose tissue IL1RN mRNA expression correlates positively with macrophage recruitment markers [13]. The expression of IL1RN was also upregulated in the adipose tissue of mice with diet-induced obesity, and IL-1Ra could reduce insulin sensitivity in rats by decreasing glucose uptake [21]. Conversely, it has been reported that IL-1RA overexpression in transgenic mice leads to fat redistribution and enhanced insulin sensitivity [22]. This apparent paradox suggests that IL1RN upregulation in obesity may reflect a complex interplay between compensatory anti-inflammatory responses and dysregulated IL-1 signaling. The concurrent upregulation of both CXCL3 and IL1RN in obese adipose tissue supports the notion that they represent components of a coordinated inflammatory program in obesity-associated adipose tissue dysfunction, though the precise mechanistic contributions of each require further investigation.

A notable computational observation of our study is the enrichment of both candidate genes in MHC class II-related programs. GSEA suggested that IL1RN was enriched in MHC class II antigen presentation, and virtual knockout of either CXCL3 or IL1RN perturbed MHC class II receptor activity-related gene programs. Antigen processing and presentation constitute the cornerstone of adaptive immunity, bridging innate immune recognition and T/B cell-mediated specific immune responses [23]. During the early stages of high-fat diet-induced obesity, MHC class II expression on adipocytes is rapidly up-regulated, enabling antigen presentation to activate $CD4^+$ T cells. Notably, MHC class II knockout significantly attenuates adipose tissue inflammation and insulin resistance, indicating that MHC-II antigen presentation may represent an early event in obesity-induced adipose inflammation [24]. Because mature adipocytes are largely absent from the stromal vascular fraction profiled in this study, the adipocyte-related observations above are cited as background and were not directly tested in our dataset. These computational data suggest a possible association between CXCL3/IL1RN-linked macrophage programs and adipose antigen presentation; however, no tissue-level co-localization or functional perturbation was performed in this study, and even co-localization would not by itself demonstrate regulation [25]. Furthermore, adipocyte hypertrophy, rather than general obesity, constitutes the principal factor driving adipose tissue inflammation and insulin resistance, as these enlarged adipocytes possess the capacity to act directly as antigen-presenting cells, thereby activating pro-inflammatory $CD4^+$ T cells and facilitating the secretion of IFN-γ [26]. The computational convergence of CXCL3 and IL1RN on MHC-II-related pathways raises the possibility, which remains to be tested, that these candidate genes may be involved in adaptive immune responses in obesity. CXCL3, by recruiting leukocytes, may amplify the pool of antigen-experienced immune cells within adipose tissue, while IL1RN, through modulation of IL-1 signaling, may regulate the threshold for T cell activation and macrophage–T cell crosstalk. This hypothetical dual involvement, if experimentally confirmed, would support further investigation of antigen presentation in obesity-associated insulin resistance; at present, it should not be interpreted as established regulation or as validated therapeutic targets.

Our network analysis predicted hsa-miR-34a-5p as a potential upstream regulator of both IL1RN and CXCL3. The network also included predicted links between MTF1 and each of the two candidate genes. Previous studies reported increased miR-34a expression in the adipose tissue of individuals with obesity and mice with diet-induced obesity [27,28]. Exosomes derived from mature adipocytes have been shown to transfer miR-34a to macrophages, where it inhibits M2 macrophage polarization and contributes to adipose inflammation and metabolic dysregulation in obesity [29]. In children with obesity, circulating miR-34a levels were positively correlated with serum TNF-α levels [30]. These studies provide context for investigating miR-34a in adipose inflammation. The proposed hsa-miR-34a-5p-CXCL3/IL1RN axis remains hypothetical. Whether hsa-miR-34a-5p directly targets either transcript, the direction of any regulatory effect, and whether such effects occur in adipose tissue macrophages require experimental validation.

Adipose tissue macrophages play a critical role in regulating adipose tissue inflammation and the development of insulin resistance in obesity [31]. Our Scissor analysis identified macrophages as the cell type most strongly associated with insulin resistance, and subsequent subpopulation analysis revealed that MAMs accounted for the highest proportion among the six macrophage subsets. MAMs represent a metabolically induced macrophage phenotype generated under exposure to high levels of glucose, insulin, and palmitate [10], conditions that closely mimic the metabolic milieu of obese adipose tissue. Nutrient availability, particularly glucose and lipids, can shift macrophage polarization toward pro- or anti-inflammatory states. Persistent metabolic stress can favor pro-inflammatory macrophage states, sustain inflammatory mediator release, and aggravate tissue injury, insulin resis-

tance, and systemic metabolic imbalance [32]. MAMs have been shown to increase adipose tissue inflammation by upregulating inflammatory markers and genes involved in lipid metabolism during HFD-induced obesity [10]. The relatively high abundance of MAMs in this dataset suggests that they may constitute a metabolically activated state that merits prioritized validation in obese adipose tissue, although their causal contribution to insulin resistance requires confirmation by functional experiments.

Cell–cell communication analysis revealed that macrophages selectively communicated with ASP via the SPP1-CD44 ligand-receptor pair. SPP1 is a secreted phosphoprotein upregulated in obesity and has been implicated in adipose tissue inflammation and fibrosis [33]. The SPP1-CD44 axis may represent a key communication channel through which macrophages influence ASP function and contribute to the metabolic dysregulation characteristic of insulin resistance. Additionally, metabolic pathway analysis revealed enrichment of amino acid metabolic pathways, including glycine, serine, and threonine metabolism, in specific macrophage subclusters. Amino acid metabolic pathways can reshape the inflammatory and reparative functional states of macrophages [34]. Serine, glycine, and threonine are closely linked to one-carbon metabolism, which can influence macrophage polarization through one-carbon flux, methyl donor supply, and redox balance, resulting in threshold regulation of inflammatory transcription and shifts in phenotypic stability [35]. The enrichment of these pathways in early-to-intermediate differentiation stages of macrophages suggests that metabolic reprogramming may be coupled to macrophage differentiation and functional polarization in obese adipose tissue, representing an additional layer of regulation that warrants further investigation. SPP1-CD44-mediated macrophage-ASP communication may cooperate with serine metabolic reprogramming to sustain inflammatory states, although this directional link requires flux analysis and receptor-blockade experiments.

The present study applied the Scissor algorithm to metabolic disease; integrating bulk insulin resistance phenotypes with adipose tissue scRNA-seq data represents a methodological extension that links cellular heterogeneity with clinical metabolic outcomes. The inclusion of single-cell virtual knockout analysis provided perturbation-based computational support for candidate gene-associated programs beyond conventional enrichment analyses. Meanwhile, examination of candidate gene expression in HFD-induced obese mice provided mRNA-level support for the bioinformatics findings. However, it is important to recognize several limitations in the present study. First, the bioinformatic analyses utilized data exclusively from publicly available databases, which lack comprehensive clinical information such as detailed metabolic parameters, medication history, and dietary habits, limiting the ability to establish direct clinical correlations with the identified candidate genes. Second, while bioinformatics approaches can reveal statistical associations and generate mechanistic hypotheses, they cannot establish biological causality. The correlations identified between candidate genes, pathways, and immune cells require functional validation through in vitro and in vivo experiments, including candidate gene overexpression/knockdown studies in macrophages and assessment of their effects on insulin signaling. Third, the single-cell dataset was derived from a limited number of samples, which may introduce sampling bias, and it profiled the stromal vascular fraction, so mature adipocytes were not represented, and adipocyte-specific mechanisms could not be assessed directly. Fourth, macrophage-specific expression of CXCL3 and IL1RN was inferred from the overlap with macrophage module genes and from xCell deconvolution, rather than measured directly in sorted macrophages. Fifth, the virtual knockout analysis, while informative, is based on computational perturbation and does not capture the full complexity of gene knockout effects in vivo. Moreover, the animal experiment examined candidate gene expression but did not directly assess insulin sensitivity or test gene-specific perturbation effects. Furthermore, immunofluorescence quantification was performed across entire image fields rather

than within segmented F4/80-positive cells; therefore, the observed staining differences could not be attributed specifically to macrophages. In addition, the MHC class II-related convergence was derived from GSEA and virtual knockout analyses; no immunostaining or immunohistochemical co-localization of MHC class II with F4/80, CXCL3, or IL1RN was performed in mouse or human adipose tissue, and no macrophage-specific perturbation or $CD4^+$T cell activation assay was conducted. Even future co-localization findings would not, on their own, establish a regulatory relationship. Therefore, the MHC class II-related findings should be regarded as computational, hypothesis-generating evidence rather than a confirmed antigen-presentation mechanism. In addition, we did not analyze our own clinical cohort; therefore, confounding by age, sex, medication, and diabetes status cannot be excluded, and whether the expression changes in CXCL3 and IL1RN are specific to insulin resistance rather than to obesity or to inflammation in general remains to be determined. Two independent cohorts with HOMA-IR-defined groups were used for external validation, but the differences were not uniformly significant (IL1RN was significant in one cohort and showed a non-significant trend in the other, and CXCL3 showed non-significant trends in both), so the specificity of these markers for insulin resistance remains to be established in larger, clinically better-characterized cohorts, and only male mice were examined, so sex-specific effects were not assessed. Despite these limitations, the multi-dimensional analytical framework employed in this study provides a systematic perspective on the candidate genes, pathways, and cellular mechanisms underlying obesity-related insulin resistance, generating testable hypotheses for future experimental studies.

4. Materials and Methods

4.1. Data Source

Insulin resistance and obesity datasets were obtained from the Gene Expression Omnibus (GEO) database. The GSE20950 dataset (platform: GPL570), including 9 adipose tissue samples from insulin-resistant subjects and 10 adipose tissue samples from insulin-sensitive subjects, was used only as the IR phenotype reference for Scissor-guided mapping of single-cell data and was not used for bulk feature gene identification. The GSE162653 dataset (platform: GPL11154) was used as the discovery dataset for obesity status, including 20 subcutaneous adipose tissue samples from obese patients and 20 subcutaneous adipose tissue samples from normal subjects. The GSE152991 dataset (platform: GPL24676) was used as the validation dataset for metabolic health status among obese individuals, including 20 subcutaneous adipose tissue samples from metabolically unhealthy obese patients and 14 subcutaneous adipose tissue samples from metabolically healthy obese subjects. Thus, GSE162653 and GSE152991 assess obesity and metabolic health status, respectively, rather than insulin resistance per se; the three datasets therefore probe different phenotype dimensions rather than providing repeated validation of the same comparison. In addition, the GSE129363 dataset (platform: GPL24676) was used as the scRNA-seq dataset, and 13 subcutaneous adipose tissue samples from obese patients were selected from this dataset. Two additional datasets were used for external validation in insulin-resistant states: GSE101492 (platform: GPL20265), abdominal subcutaneous white adipose tissue from 80 obese women selected from the extremes of HOMA-IR (40 insulin-sensitive and 40 insulin-resistant) [36]; and GSE174475 (platform: GPL18573), purified subcutaneous adipocytes from 43 individuals in the first and fourth HOMA-IR quartiles (16 insulin-sensitive and 27 insulin-resistant) [37].

4.2. Single-Cell Analysis

The Seurat package (v 5.1.0) was utilized for the quality control of GSE129363 dataset [38]. The selection criteria were defined as follows: the number of genes quantified

per cell (nFeature_RNA) was required to be between 200 and 4000; the total gene counts per cell (nCount_RNA) was constrained to lie within the range of 3 to 30,000; and the proportion of mitochondrial gene expression per cell (percent.mt) was limited not to exceed 15%. The NormalizeData function was employed to standardize the data, followed by the FindVariableFeatures function to identify the top 2000 highly variable genes (HVGs). The results were visualized via the VariableFeaturePlot function to highlight the top 10 HVGs. All samples in the single-cell dataset were scaled using the ScaleData function. The RunPCA function was applied to perform principal component analysis (PCA) on the HVGs. The ElbowPlot function from the Seurat package (v 5.1.0) was used to select the appropriate principal components (PCs). Initially, cell clustering was conducted utilizing the FindNeighbors and FindClusters functions. Following this, dimensionality reduction was achieved through uniform manifold approximation and projection (UMAP) with a resolution parameter set at 0.75. Subsequently, cell type annotation was performed by applying marker genes from the literature 37. Because GSE129363 profiled the stromal vascular fraction of adipose tissue [39], the adipocyte-like clusters (0, 2, 3 and 10) were re-examined with adipose progenitor/stromal markers (CFD, MGP, APOD, CXCL14 and WISP2) and with mature adipocyte markers (ADIPOQ, PLIN1 and CIDEC); high expression of the progenitor/stromal markers and negligible expression of the mature adipocyte markers supported annotation as adipose stromal/progenitor cells (ASP). The following markers were used: CFD, MGP, APOD, CXCL14 and WISP2 for ASP; CD163, SLC11A1 and MAFB for macrophages; EGFLAM, STEAP4 and RGS5 for pericytes; IL7R and CD3D for T cells; MS4A1 and CD79A for B cells. The expression patterns of these marker genes were then visualized using a dot plot.

Finally, to screen for cells associated with the insulin resistance phenotype at the single-cell level, the Scissor package (v 2.0.0) [11] was used in combination with the expression matrix of the GSE20950 dataset. The percentage of cells labeled "+" in the screening results relative to the total number of cells in each cell subset was calculated separately, and the cell subset with the highest percentage was defined as insulin resistance-related cells, namely key cells.

4.3. High-Dimensional Weighted Gene Co-Expression Network Analysis (hdWGCNA)

The dimensionality reduction and clustering techniques applied to the key cells were consistent with those described in Section 4.2, utilizing a resolution parameter of 0.75. The key cells were divided into distinct subclusters. To identify co-expression module genes associated with key cells in obesity, hdWGCNA was performed on key cells from the GSE129363 dataset using the hdWGCNA package (v 0.4.00) [40]. The setupForWGCNA function was used to construct the hdWGCNA object with the parameter fraction = 0.05, selecting genes that are expressed in a minimum of 5% of the cell population. The MetacellsByGroups function was applied with default parameters (k = 25, max_shared = 10) to convert the object into a metacell object. Subsequently, the TestSoftPowers function was utilized to perform parameter scanning in order to identify the optimal soft threshold (power) for the construction of the co-expression network. By analyzing the network topology across varying power levels and calculating the soft threshold (power) and the scale-free fitting index, the soft threshold ($R^2 > 0.8$) was selected, which both preserved strong gene-gene correlation in the adjacency matrix and eliminated weak connections. This threshold was used to construct the scale-free network with the topological overlap matrix (TOM). The ConstructNetwork function was employed to develop the co-expression network based on the optimal soft threshold (power). The ModuleEigengenes function was used to calculate the module eigengenes (MEs) for each co-expression module. Additionally, the ModuleConnectivity function was utilized to calculate the eigengene-based connectivity (kME) for

individual genes within each co-expression module. Finally, the ModuleExprScore function was used to calculate the scores of module genes, and dot plots were plotted to display the expression profiles of module genes across different modules. Modules with higher scores in key cell types were designated as key modules, and the top 100 genes in these modules were selected as key module genes and subjected to subsequent analyses.

4.4. Pseudotime Analysis

Key cell populations were classified into distinct subclusters according to marker genes. The annotated results were visualized using UMAP plots, and stacked bar charts were applied to show the proportion of each key subcluster within the main cell populations. UMAP plots were applied to display key cell subsets and integrated cellular populations. In addition, single-cell samples from patients with obesity were divided into diabetic and non-diabetic groups based on diabetic status. Stacked bar charts were used to show the proportion of each cell type in the two groups. To explore the differentiation status and trajectory of key cells, pseudotime analysis was carried out using the Monocle package (v 2.28.0) [41]. The plot_genes_in_pseudotime function was used to investigate the expression patterns of key module genes throughout cell differentiation.

4.5. Exploration of Cellular Functions from Multiple Perspectives

Using the CellChat package (v 1.6.1) [42], intercellular communication networks across cell types were inferred for samples in the GSE129363 dataset. Calculations were performed to identify potential ligand-receptor interactions and signaling between different cell types. Additionally, the scMetabolism package (v 0.2.1) [43] was used to calculate the metabolic pathway activity score for each cell.

4.6. Identification of Hub Genes

The DESeq2 package (v 1.40.2) [44] was utilized to identify bulk differentially expressed genes (DEGs) between the obesity and control groups in the GSE162653 dataset, with thresholds set at $|\log_2 FC| > 1$ and $p < 0.05$. According to the $\log_2$ FC values, the top 5 upregulated and top 5 downregulated bulk DEGs were labeled and visualized. The ggvenn package (v 0.1.10) [45] was used to identify the intersection between bulk DEGs and key module genes, which were defined as overlapping genes. Moreover, a network of protein–protein interactions (PPI) was created from the overlapping genes using the Search Tool for the Retrieval of Interacting Genes/Proteins (STRING) database (https://string-db.org/, accessed on 12 January 2026) (confidence score ≥ 0.4). Finally, the MCODE algorithm was applied to screen overlapping genes, and the 12 genes of the top-ranked module were selected as hub genes for subsequent analyses.

4.7. Feature Gene Identification

To further screen feature genes, the 12 hub genes were used as input to three different machine learning algorithms. In the GSE162653 dataset, the Boruta package (v 8.0.0) [46] was applied to screen the 12 hub genes, and genes identified as "Confirmed" were designated as Boruta genes. The caret package (v 6.0-94) [47] was used to screen overlapping genes using the support vector machine recursive feature elimination (SVM-RFE) algorithm. The first gene set with the highest accuracy was identified and defined as SVM-RFE genes. Additionally, the randomForest package (v 4.7-1.2) [48] was applied to develop the random forest (RF) model. The number of decision trees was set to 500, and the number of features considered for node splitting was defined as the square root of the total number of genes. The out-of-bag (OOB) error rate was monitored as the number of trees increased to evaluate model convergence. Finally, the top 5 genes ranked by importance were selected as RF genes

using 5-fold cross-validation. Feature genes were defined as the intersection of Boruta genes, SVM-RFE genes, and RF genes using the ggvenn package (v 0.10). Finally, the Wilcoxon test ($p < 0.05$) was employed to compare the expression levels of the feature genes between the groups compared in the GSE162653 and GSE152991 datasets. Among the feature genes, those showing statistically significant differential expression with consistent trends across both datasets were retained as candidate genes.

4.8. Gene Set Enrichment Analysis (GSEA)

The reference gene set was obtained from the "c2.cp.all.v2022.1.Hs.symbols.gmt" file in the Molecular Signatures Database (MSigDB) (https://www.gsea-msigdb.org/gsea/msigdb, accessed on 13 January 2026). GSEA was performed using the clusterProfiler package (v 4.15.0.003) [49] to identify enriched pathways. The psych package (v 2.4.6.26) was used to compute the correlation coefficients between each candidate gene and all genes in the GSE162653 dataset [50]. These correlation coefficients were arranged in descending order to produce a ranked list of genes associated with each candidate gene (|normalized enrichment score (NES)| > 1, false discovery rate (FDR) < 0.25, and $p < 0.05$). The top 5 pathways were displayed by *p*-value.

4.9. Virtual Knockout (KO) Analysis of Candidate Genes in Single Cells

In the key cells of the GSE129363 dataset, the scTenifoldKnk algorithm (v 1.0.2) [14] was used to perform virtual KO analysis on the candidate genes individually, resulting in the acquisition of affected genes ($p < 0.05$). Enrichment analysis of the impacted genes was conducted utilizing the clusterProfiler package.

4.10. Immune Microenvironment Analysis

In the GSE162653 dataset, immune cell enrichment was estimated using the xCell algorithm (v 1.1.0). xCell enrichment scores were obtained for 34 immune cell types across samples. The Wilcoxon test was used to compare xCell enrichment scores between the obesity and control groups and to identify cell types with significant between-group differences ($p < 0.05$). Next, Spearman correlation analysis was performed via the psych package (v 2.4.6.26) to explore associations between differentially expressed immune cells themselves, as well as between candidate genes and differentially expressed immune cells ($p < 0.05$ and |cor| > 0.30).

4.11. Exploring the Potential Functions of Candidate Genes from Multiple Perspectives

The miRNet database (https://www.mirnet.ca/, accessed on 17 January 2026) [51] was used to predict microRNAs (miRNAs) associated with the candidate genes. Moreover, the ChEA3 database (https://amp.pharm.mssm.edu/chea3/, accessed on 17 January 2026) [52] was used to acquire transcription factors (TFs) linked to candidate genes. The top 10 ranked TFs were selected as key TFs. Finally, the miRNA-mRNA-TF regulatory network was visualized.

4.12. Enrichment Analysis of Macrophage-Associated Genes

Macrophages were extracted from the single-cell RNA sequencing data. Based on the expression of candidate genes, macrophages were stratified by transcript detection (expression value > 0 vs. 0) rather than by a biological high/low threshold, and this comparison is therefore exploratory. Subsequently, the FindMarkers function was used to identify DEGs between macrophages with and without detectable expression using the Wilcoxon rank-sum test. The screening thresholds were set as adj. $p < 0.05$ and avg_$\log_2$FC > 0.25 to identify significantly upregulated DEGs. All genes were sorted in descending order according to the

avg_log$_2$FC values obtained from the differential expression analysis. C2.all.v2023.2.Hs.symbols.gmt was downloaded from the MSigDB database as the reference gene set, and the clusterProfiler package was used to perform gene enrichment analysis.

4.13. Animals

Male 5-week-old C57BL/6J mice, purchased from Shanghai Model Organisms Center (Shanghai, China), were maintained under a standard 12 h light/dark cycle with food and water freely available. Following a one-week acclimation period, mice were randomly allocated into either a normal diet (ND; D12450J, 10% kcal from fat; Research Diets, Inc., New Brunswick, NJ, USA) group ($n = 3$) or a high-fat diet (HFD; D12492, 60% kcal from fat; Research Diets, Inc., New Brunswick, NJ, USA) group ($n = 4$). After 24 weeks, mice were starved overnight and anesthetized. Epididymal adipose tissue samples were collected, rapidly frozen in liquid nitrogen, and subsequently stored at a temperature of −80 °C. The animal was considered the biological replicate; sections and fields were not treated as independent biological replicates.

4.14. RT-qPCR

Total RNA was extracted from the adipose tissue using AG RNAex Pro RNA Reagent (AG21102, Accurate Biology, Changsha, China) in accordance with the guidelines provided by the manufacturer. Reverse transcription was performed using the reverse transcription reagent with Evo M-MLV RTase (AG11706, Accurate Biology, Changsha, China). qPCR was performed using SYBR Green Pro Taq HS (AG11702, Accurate Biology, Changsha, China) on a LightCycler 480 II real-time PCR system (Roche, Basel, Switzerland) to quantify the mRNA expression levels of *IL1RN* and *CXCL3*. Relative gene expression was calculated using the $2^{-\Delta\Delta Ct}$ method, with β-actin as the internal reference. All primers were synthesized by Guangzhou Baiweining Biotechnology Co., Ltd. (Guangzhou, China), and their sequences are provided in Supplementary Table S1.

4.15. Immunofluorescent Staining

Paraffin-embedded adipose tissue sections were deparaffinized with xylene and rehydrated through graded ethanol solutions prepared from absolute ethanol (analytical grade, Guangzhou Chemical Reagent Factory, Guangzhou, China). Heat-induced antigen retrieval was performed using EDTA buffer. After blocking with bovine serum albumin (BSA), the sections were incubated overnight at 4 °C in the dark with primary antibodies against CXCL3 (ab220431, Abcam, Cambridge, UK), IL-1RA (31127-1-AP, Proteintech, Wuhan, China), and F4/80 (ab6640, Abcam, Cambridge, UK). After washing with TBST, the sections were incubated with Alexa Fluor 555-conjugated goat anti-rabbit IgG (ab150078, Abcam, Cambridge, UK) and Alexa Fluor 488-conjugated goat anti-rat IgG (ab150165, Abcam, Cambridge, UK) secondary antibodies. The sections were mounted in DAPI Fluoromount-G (0100-20, SouthernBiotech, Birmingham, AL, USA) for nuclear counterstaining. For each animal, two sections were analyzed, and five randomly selected fields per section were imaged using a Leica DMi8 automated inverted microscope (Leica Microsystems, Wetzlar, Germany) at 400× total magnification (40× objective). F4/80 signals were detected in the Alexa Fluor 488 channel (green). Merged fluorescence images were used to qualitatively assess the spatial distribution of IL-1RA and CXCL3 signals relative to F4/80-positive cells. Mean fluorescence intensity was quantified across the entire image field using ImageJ (v 1.54p) with automatic thresholding (Default algorithm), rather than within segmented F4/80-positive regions. Measurements across all fields were averaged for each animal to obtain a single value per biological replicate for group comparisons.

4.16. Biostatistical Analysis

Bioinformatics analyses were performed in R (v 4.2.2, R Foundation for Statistical Computing, Vienna, Austria). Between-group comparisons of bioinformatic data were performed using the Wilcoxon test. RT-qPCR results were presented as mean ± standard deviation, and comparisons between groups were conducted using a *t*-test. For immunofluorescence quantification, the animal was used as the unit of analysis: the mean value across all examined fields was calculated for each animal, and group comparisons were performed using a t-test on these animal-level means. Statistical significance was defined as $p < 0.05$.

4.17. External Validation in Independent Cohorts

CXCL3 and IL1RN expression was compared between insulin-resistant and insulin-sensitive groups in GSE101492 and GSE174475 using the Wilcoxon test, and $p < 0.05$ was considered statistically significant. Each dataset was analyzed separately, without cross-dataset normalization.

5. Conclusions

In conclusion, this study identifies CXCL3 and IL1RN as macrophage-associated candidate genes linked to adipose inflammation and metabolic dysfunction in obesity, with possible associations with insulin resistance that require further validation. The limited external validation evidence does not establish their specificity for insulin resistance. MAMs were identified as the most abundant macrophage subset. The computational enrichment of both candidate genes in MHC class II-related programs raises a hypothesis of a possible association between these candidate genes and MHC class II-related immune programs in obese adipose tissue; this hypothesis requires tissue-level co-localization and functional validation and should not be regarded as an established antigen-presentation mechanism. These findings provide a framework for further mechanistic investigation and suggest the miR-34a-CXCL3/IL1RN axis as a candidate regulatory pathway. Further functional validation of these candidate genes and their regulatory networks in experimental models will be essential to translate these findings into clinical applications.

Supplementary Materials: The following supporting information can be downloaded at: https://www.mdpi.com/article/10.3390/ijms272310542/s1.

Author Contributions: Conceptualization, K.Y. and Y.G.; methodology, K.Y. and X.Z.; software, X.Z. and H.Y.; validation, K.Y., X.Z., and G.Y.; formal analysis, G.Y. and X.Z.; investigation, G.Y.; resources, C.L.; data curation, J.L. and L.S.; in vivo experiment, W.H. and M.D.; writing—original draft preparation, K.Y. and X.Z.; writing—review and editing, G.Y. and Y.G.; visualization, C.L., J.L., and L.S.; supervision, Y.G.; project Administration, Y.G.; funding acquisition, K.Y. and Y.G. All authors have read and agreed to the published version of the manuscript.

Funding: This research was funded by the Guangdong Basic and Applied Basic Research Foundation (Grant No. 2023A1515110726, No.2026A1515012595), the Guangdong Medical Research Foundation (Grant No. A2024544), the Guangzhou Basic and Applied Basic Research Foundation (Grant No. 2025A04J5293), and the National Natural Science Foundation of China (Grant No. 82200881).

Institutional Review Board Statement: This investigation is a secondary analysis of publicly deposited, de-identified transcriptomic datasets (GSE20950, GSE162653, GSE152991, GSE129363, GSE101492 and GSE174475) retrieved from the NCBI Gene Expression Omnibus. All original datasets were collected, anonymized, and deposited by their respective submitting investigators in accordance with the ethical requirements of their respective institutional review boards. The animal experiments were carried out in accordance with the guidelines for the care and use of laboratory animals. The animal experiment protocols were approved by the Clinical Research and Laboratory Animal Ethics Committee, The First Affiliated Hospital of Sun Yat-sen University ([2024] number 150).

Informed Consent Statement: Not applicable.

Data Availability Statement: The datasets presented in this study are available in online repositories. The names of the repositories and accession numbers are provided in the Section 4 (GSE20950, GSE162653, GSE152991, GSE129363, GSE101492 and GSE174475). Additional data supporting the conclusions of this study will be made available by the authors upon reasonable request.

Acknowledgments: We thank all participants for their advice and support of this study. All individuals have consented to the acknowledgment.

Conflicts of Interest: The authors declare no conflicts of interest.

Abbreviations

The following abbreviations are used in this manuscript:

ASP	adipose stromal/progenitor cells
ATMs	adipose tissue macrophages
CLS	crown-like structure macrophages
CXCL3	C-X-C motif chemokine 3
DEGs	differentially expressed genes
FDR	false discovery rate
GEO	Gene Expression Omnibus
GO	Gene Ontology
GSEA	Gene Set Enrichment Analysis
hdWGCNA	High-dimensional weighted gene co-expression network analysis
HFD	High-fat diet
HOMA-IR	homeostasis model assessment of insulin resistance
HVGs	highly variable genes
IL-1RA	Interleukin-1 receptor antagonist
IL1RN	interleukin-1 receptor antagonist (gene)
IR	Insulin resistance
KEGG	Kyoto Encyclopedia of Genes and Genomes
kME	eigengene-based connectivity
KO	knockout
LAMs	lipid-associated macrophages
MAMs	metabolically activated macrophages
MCODE	molecular complex detection
MEs	module eigengenes
MHC	major histocompatibility complex
miRNAs	microRNAs
MSigDB	Molecular Signatures Database
NAMs/SAMs	sympathetic neuron-associated macrophages
ND	Normal diet
NES	normalized enrichment score
OOB	out-of-bag
PCA	principal component analysis
PCs	principal components
PPI	protein–protein interaction
ProMac	proliferative macrophages
RF	random forest
RT-qPCR	reverse transcription quantitative real-time PCR
scRNA-seq	single-cell RNA sequencing
SPP1	secreted phosphoprotein 1
SVM-RFE	support vector machine recursive feature elimination
TFs	transcription factors
TOM	topological overlap matrix
UMAP	uniform manifold approximation and projection
VAM	vascular-associated macrophages

References

1. Chakaroun, R.M.; Pradhan, M.; Bjornson, E.; Arvidsson, D.; Fridolfsson, J.; Gummesson, A.; Schoeler, M.; Mitteregger, M.; Smith, G.J.; Larsson, I.; et al. Multi-omic definition of metabolic obesity through adipose tissue-microbiome interactions. *Nat. Med.* **2026**, *32*, 113–125. [CrossRef] [PubMed]
2. Perdomo, C.M.; Cohen, R.V.; Sumithran, P.; Clement, K.; Fruhbeck, G. Contemporary medical, device, and surgical therapies for obesity in adults. *Lancet* **2023**, *401*, 1116–1130. [CrossRef] [PubMed]
3. GBD 2021 Adult BMI Collaborators. Global, regional, and national prevalence of adult overweight and obesity, 1990–2021, with forecasts to 2050: A forecasting study for the Global Burden of Disease Study 2021. *Lancet* **2025**, *405*, 813–838. [CrossRef] [PubMed]
4. Heymsfield, S.B.; Wadden, T.A. Mechanisms, Pathophysiology, and Management of Obesity. *N. Engl. J. Med.* **2017**, *376*, 254–266. [CrossRef] [PubMed]
5. Choo, Y.N.; Ravi, R.N.; Subramaniyan, V. Insulin resistance induced by obesity: Mechanisms, metabolic implications and therapeutic approaches. *Mol. Biol. Rep.* **2026**, *53*, 357. [CrossRef] [PubMed]
6. Hagberg, C.E.; Spalding, K.L. White adipocyte dysfunction and obesity-associated pathologies in humans. *Nat. Rev. Mol. Cell Biol.* **2024**, *25*, 270–289. Correction in *Nat. Rev. Mol. Cell Biol.* **2024**, *25*, 333. [CrossRef] [PubMed]
7. Zatterale, F.; Longo, M.; Naderi, J.; Raciti, G.A.; Desiderio, A.; Miele, C.; Beguinot, F. Chronic Adipose Tissue Inflammation Linking Obesity to Insulin Resistance and Type 2 Diabetes. *Front. Physiol.* **2019**, *10*, 1607. [CrossRef] [PubMed]
8. Jaitin, D.A.; Adlung, L.; Thaiss, C.A.; Weiner, A.; Li, B.; Descamps, H.; Lundgren, P.; Bleriot, C.; Liu, Z.; Deczkowska, A.; et al. Lipid-Associated Macrophages Control Metabolic Homeostasis in a Trem2-Dependent Manner. *Cell* **2019**, *178*, 686–698.e14. [CrossRef] [PubMed]
9. Pirzgalska, R.M.; Seixas, E.; Seidman, J.S.; Link, V.M.; Sanchez, N.M.; Mahu, I.; Mendes, R.; Gres, V.; Kubasova, N.; Morris, I.; et al. Sympathetic neuron-associated macrophages contribute to obesity by importing and metabolizing norepinephrine. *Nat. Med.* **2017**, *23*, 1309–1318. [CrossRef] [PubMed]
10. Coats, B.R.; Schoenfelt, K.Q.; Barbosa-Lorenzi, V.C.; Peris, E.; Cui, C.; Hoffman, A.; Zhou, G.; Fernandez, S.; Zhai, L.; Hall, B.A.; et al. Metabolically Activated Adipose Tissue Macrophages Perform Detrimental and Beneficial Functions during Diet-Induced Obesity. *Cell Rep.* **2017**, *20*, 3149–3161. [CrossRef] [PubMed]
11. Sun, D.; Guan, X.; Moran, A.E.; Wu, L.Y.; Qian, D.Z.; Schedin, P.; Dai, M.S.; Danilov, A.V.; Alumkal, J.J.; Adey, A.C.; et al. Identifying phenotype-associated subpopulations by integrating bulk and single-cell sequencing data. *Nat. Biotechnol.* **2022**, *40*, 527–538. [CrossRef] [PubMed]
12. Bao, Y.; Tong, C.; Xiong, X. CXCL3: A key player in tumor microenvironment and inflammatory diseases. *Life Sci.* **2024**, *348*, 122691. [CrossRef] [PubMed]
13. Fruhbeck, G.; Catalan, V.; Ramirez, B.; Valenti, V.; Becerril, S.; Rodriguez, A.; Moncada, R.; Baixauli, J.; Silva, C.; Escalada, J.; et al. Serum Levels of IL-1 RA Increase with Obesity and Type 2 Diabetes in Relation to Adipose Tissue Dysfunction and are Reduced After Bariatric Surgery in Parallel to Adiposity. *J. Inflamm. Res.* **2022**, *15*, 1331–1345. [CrossRef] [PubMed]
14. Osorio, D.; Zhong, Y.; Li, G.; Xu, Q.; Yang, Y.; Tian, Y.; Chapkin, R.S.; Huang, J.Z.; Cai, J.J. scTenifoldKnk: An efficient virtual knockout tool for gene function predictions via single-cell gene regulatory network perturbation. *Patterns* **2022**, *3*, 100434. [CrossRef] [PubMed]
15. Ahmed, B.; Sultana, R.; Greene, M.W. Adipose tissue and insulin resistance in obese. *Biomed. Pharmacother.* **2021**, *137*, 111315. [CrossRef] [PubMed]
16. Huang, L.Y.; Chiu, C.J.; Hsing, C.H.; Hsu, Y.H. Interferon Family Cytokines in Obesity and Insulin Sensitivity. *Cells* **2022**, *11*, 4041. [CrossRef] [PubMed]
17. Dinarello, C.A. Overview of the IL-1 family in innate inflammation and acquired immunity. *Immunol. Rev.* **2018**, *281*, 8–27. [CrossRef] [PubMed]
18. Li, X.; Ren, Y.; Chang, K.; Wu, W.; Griffiths, H.R.; Lu, S.; Gao, D. Adipose tissue macrophages as potential targets for obesity and metabolic diseases. *Front. Immunol.* **2023**, *14*, 1153915. [CrossRef] [PubMed]
19. Hildreth, A.D.; Ma, F.; Wong, Y.Y.; Sun, R.; Pellegrini, M.; O'Sullivan, T.E. Single-cell sequencing of human white adipose tissue identifies new cell states in health and obesity. *Nat. Immunol.* **2021**, *22*, 639–653. [CrossRef] [PubMed]
20. He, X.; Wang, L.; Li, H.; Liu, Y.; Tong, C.; Xie, C.; Yan, X.; Luo, D.; Xiong, X. CSF2 upregulates CXCL3 expression in adipocytes to promote metastasis of breast cancer via the FAK signaling pathway. *J. Mol. Cell Biol.* **2023**, *15*, mjad025. [CrossRef] [PubMed]
21. Somm, E.; Cettour-Rose, P.; Asensio, C.; Charollais, A.; Klein, M.; Theander-Carrillo, C.; Juge-Aubry, C.E.; Dayer, J.M.; Nicklin, M.J.; Meda, P.; et al. Interleukin-1 receptor antagonist is upregulated during diet-induced obesity and regulates insulin sensitivity in rodents. *Diabetologia* **2006**, *49*, 387–393. [CrossRef] [PubMed]
22. Wong, M.L.; Mastronardi, C.; Paz-Filho, G.; Simeonovic, C.; Licinio, J. Varying levels of interleukin 1 receptor antagonist (Il1rn) gene expression affect circulating leptin concentrations and fat distribution. *Genom. Psychiatry* **2025**, *1*, 74–75. [CrossRef] [PubMed]

23. Pishesha, N.; Harmand, T.J.; Ploegh, H.L. A guide to antigen processing and presentation. *Nat. Rev. Immunol.* **2022**, *22*, 751–764. [CrossRef] [PubMed]
24. Deng, T.; Lyon, C.J.; Minze, L.J.; Lin, J.; Zou, J.; Liu, J.Z.; Ren, Y.; Yin, Z.; Hamilton, D.J.; Reardon, P.R.; et al. Class II major histocompatibility complex plays an essential role in obesity-induced adipose inflammation. *Cell Metab.* **2013**, *17*, 411–422. [CrossRef] [PubMed]
25. Bolte, S.; Cordelieres, F.P. A guided tour into subcellular colocalization analysis in light microscopy. *J. Microsc.* **2006**, *224*, 213–232. [CrossRef] [PubMed]
26. Xiao, L.; Yang, X.; Lin, Y.; Li, S.; Jiang, J.; Qian, S.; Tang, Q.; He, R.; Li, X. Large adipocytes function as antigen-presenting cells to activate CD4(+) T cells via upregulating MHCII in obesity. *Int. J. Obes.* **2016**, *40*, 112–120. [CrossRef] [PubMed]
27. Ortega, F.J.; Moreno-Navarrete, J.M.; Pardo, G.; Sabater, M.; Hummel, M.; Ferrer, A.; Rodriguez-Hermosa, J.I.; Ruiz, B.; Ricart, W.; Peral, B.; et al. MiRNA expression profile of human subcutaneous adipose and during adipocyte differentiation. *PLoS ONE* **2010**, *5*, e9022. [CrossRef] [PubMed]
28. Fu, T.; Seok, S.; Choi, S.; Huang, Z.; Suino-Powell, K.; Xu, H.E.; Kemper, B.; Kemper, J.K. MicroRNA 34a inhibits beige and brown fat formation in obesity in part by suppressing adipocyte fibroblast growth factor 21 signaling and SIRT1 function. *Mol. Cell. Biol.* **2014**, *34*, 4130–4142. [CrossRef] [PubMed]
29. Pan, Y.; Hui, X.; Hoo, R.L.C.; Ye, D.; Chan, C.Y.C.; Feng, T.; Wang, Y.; Lam, K.S.L.; Xu, A. Adipocyte-secreted exosomal microRNA-34a inhibits M2 macrophage polarization to promote obesity-induced adipose inflammation. *J. Clin. Investig.* **2019**, *129*, 834–849. [CrossRef] [PubMed]
30. Lischka, J.; Schanzer, A.; Hojreh, A.; Ba-Ssalamah, A.; de Gier, C.; Valent, I.; Item, C.B.; Greber-Platzer, S.; Zeyda, M. Circulating microRNAs 34a, 122, and 192 are linked to obesity-associated inflammation and metabolic disease in pediatric patients. *Int. J. Obes.* **2021**, *45*, 1763–1772. [CrossRef] [PubMed]
31. Soedono, S.; Julietta, V.; Nawaz, H.; Cho, K.W. Dynamic Roles and Expanding Diversity of Adipose Tissue Macrophages in Obesity. *J. Obes. Metab. Syndr.* **2024**, *33*, 193–212. [CrossRef] [PubMed]
32. Kolliniati, O.; Ieronymaki, E.; Vergadi, E.; Tsatsanis, C. Metabolic Regulation of Macrophage Activation. *J. Innate Immun.* **2022**, *14*, 51–68. [CrossRef] [PubMed]
33. Nomiyama, T.; Perez-Tilve, D.; Ogawa, D.; Gizard, F.; Zhao, Y.; Heywood, E.B.; Jones, K.L.; Kawamori, R.; Cassis, L.A.; Tschop, M.H.; et al. Osteopontin mediates obesity-induced adipose tissue macrophage infiltration and insulin resistance in mice. *J. Clin. Investig.* **2007**, *117*, 2877–2888. [CrossRef] [PubMed]
34. Yin, Y.; Yan, C.; Pei, X.; Rao, J.; Wu, L.; Xue, Y.; Sun, H.; Sheng, Y. Amino acid metabolism modulates macrophage polarization: Implications for autoimmune-related diseases. *Front. Immunol.* **2026**, *17*, 1736082. [CrossRef] [PubMed]
35. Shan, X.; Hu, P.; Ni, L.; Shen, L.; Zhang, Y.; Ji, Z.; Cui, Y.; Guo, M.; Wang, H.; Ran, L.; et al. Serine metabolism orchestrates macrophage polarization by regulating the IGF1-p38 axis. *Cell. Mol. Immunol.* **2022**, *19*, 1263–1278. [CrossRef] [PubMed]
36. Gao, H.; Kerr, A.; Jiao, H.; Hon, C.C.; Ryden, M.; Dahlman, I.; Arner, P. Long Non-Coding RNAs Associated with Metabolic Traits in Human White Adipose Tissue. *eBioMedicine* **2018**, *30*, 248–260. [CrossRef] [PubMed]
37. Emont, M.P.; Jacobs, C.; Essene, A.L.; Pant, D.; Tenen, D.; Colleluori, G.; Di Vincenzo, A.; Jorgensen, A.M.; Dashti, H.; Stefek, A.; et al. A single-cell atlas of human and mouse white adipose tissue. *Nature* **2022**, *603*, 926–933. [CrossRef] [PubMed]
38. Stuart, T.; Butler, A.; Hoffman, P.; Hafemeister, C.; Papalexi, E.; Mauck, W.M., 3rd; Hao, Y.; Stoeckius, M.; Smibert, P.; Satija, R. Comprehensive Integration of Single-Cell Data. *Cell* **2019**, *177*, 1888–1902.e21. [CrossRef] [PubMed]
39. Vijay, J.; Gauthier, M.F.; Biswell, R.L.; Louiselle, D.A.; Johnston, J.J.; Cheung, W.A.; Belden, B.; Pramatarova, A.; Biertho, L.; Gibson, M.; et al. Single-cell analysis of human adipose tissue identifies depot and disease specific cell types. *Nat. Metab.* **2020**, *2*, 97–109. [CrossRef] [PubMed]
40. Morabito, S.; Reese, F.; Rahimzadeh, N.; Miyoshi, E.; Swarup, V. hdWGCNA identifies co-expression networks in high-dimensional transcriptomics data. *Cell Rep. Methods* **2023**, *3*, 100498. [CrossRef] [PubMed]
41. Trapnell, C.; Cacchiarelli, D.; Grimsby, J.; Pokharel, P.; Li, S.; Morse, M.; Lennon, N.J.; Livak, K.J.; Mikkelsen, T.S.; Rinn, J.L. The dynamics and regulators of cell fate decisions are revealed by pseudotemporal ordering of single cells. *Nat. Biotechnol.* **2014**, *32*, 381–386. [CrossRef] [PubMed]
42. Jin, S.; Guerrero-Juarez, C.F.; Zhang, L.; Chang, I.; Ramos, R.; Kuan, C.H.; Myung, P.; Plikus, M.V.; Nie, Q. Inference and analysis of cell-cell communication using CellChat. *Nat. Commun.* **2021**, *12*, 1088. [CrossRef] [PubMed]
43. Wu, Y. scMetabolism: Quantifying Metabolism Activity at the Single-Cell Resolution. Available online: https://github.com/wu-yc/scMetabolism (accessed on 29 October 2026).
44. Love, M.I.; Huber, W.; Anders, S. Moderated estimation of fold change and dispersion for RNA-seq data with DESeq2. *Genome Biol.* **2014**, *15*, 550.
45. Yan, L. ggvenn: Draw Venn Diagram by 'ggplot2'. R package. Available online: https://CRAN.R-project.org/package=ggvenn (accessed on 29 October 2026).
46. Kursa, M.B.; Rudnicki, W.R. Feature Selection with the Boruta Package. *J. Stat. Softw.* **2010**, *36*, 1–13. [CrossRef]

47. Kuhn, M. Building Predictive Models in R Using the caret Package. *J. Stat. Softw.* **2008**, *28*, 1–26.
48. Liaw, A.; Wiener, M. Classification and Regression by randomForest. *R News* **2002**, *2*, 18–22.
49. Yu, G.; Wang, L.G.; Han, Y.; He, Q.Y. clusterProfiler: An R package for comparing biological themes among gene clusters. *OMICS* **2012**, *16*, 284–287. [CrossRef] [PubMed]
50. Revelle, W. psych: Procedures for Psychological, Psychometric, and Personality Research. 2026. Available online: https://CRAN.R-project.org/package=psych (accessed on 29 October 2026).
51. Chang, L.; Zhou, G.; Soufan, O.; Xia, J. miRNet 2.0: Network-based visual analytics for miRNA functional analysis and systems biology. *Nucleic Acids Res.* **2020**, *48*, W244–W251. [CrossRef] [PubMed]
52. Keenan, A.B.; Torre, D.; Lachmann, A.; Leong, A.K.; Wojciechowicz, M.L.; Utti, V.; Jagodnik, K.M.; Kropiwnicki, E.; Wang, Z.; Ma'ayan, A. ChEA3: Transcription factor enrichment analysis by orthogonal omics integration. *Nucleic Acids Res.* **2019**, *47*, W212–W224. [CrossRef] [PubMed]

Disclaimer/Publisher's Note: The statements, opinions and data contained in all publications are solely those of the individual author(s) and contributor(s) and not of MDPI and/or the editor(s). MDPI and/or the editor(s) disclaim responsibility for any injury to people or property resulting from any ideas, methods, instructions or products referred to in the content.